An On-Body UHF RFID Tag With DDRR Antenna for Healthcare Data Streaming Applications

Jack D. Hughes, Robert Horne, Nathan Brabon, and John Batchelor, *Senior Member, IEEE*

***Abstract*—This paper describes the development of a Direct Driven Resonant Radiator (DDRR) antenna for an ultra-low power UHF RFID tag system, integrating an accelerometer for movement tracking using a passive backscattering communications link. An outline of a system intended for healthcare applications involving wireless movement detection, such as therapeutic recovery exercises is described. The tag comprises of a UHF RFID transponder connected to a 4 cm (0.115λ) diameter, 1 mm thick (0.0028λ) skin-mounted antenna. Off-body read ranges of 3.6 m with 1 kB/s data communication are achieved. The DDRR radiation pattern is a limiting factor in movement tracking, offering only limited angles of detection, which could be improved with spatial diversity in the reader antennas.**

***Index Terms*—RFID tag, RFID in healthcare, sensors and networks, antenna and design, and location, people, and object tracking.**

I. Introduction

IN RECENT years, radio-frequency identification (RFID) tags have helped make opportunities such as wireless-health monitoring obtainable in a cost-effective manner [1]. In doing so, they have propelled interest in on-body sensor networks for medical, military, and leisure applications [2]. While various mobile and wearable platforms have been developed, obtaining reliable low power data from devices placed directly on the skin remains an open challenge owing to the significant losses the body introduces. One such major factor in this research is the necessity to improve read range from an antenna on-skin. When considering on-body antenna design, a balance must be made between the desired structural performance and the radiation performance. Epidermal Electronics [3], originally proposed moving external electronics and sensors from items such as clothing, directly to the skin and set a standard to offer seamless communication from a completely unobtrusive and comfortable device. However, the RF capabilities of such devices suffer poor read range performance, since the losses are so prevalent for an antenna without shielding from the body. Outside of epidermal electronics, more traditional designs for on-body antennas overcome losses by introducing separation between the body and the antenna, low-loss rigid materials, or ground plane EBG structures [4]. Hence, the current state of the field suggests on-body antennas looking to achieve longer read distances, must compromise on structural characteristics for performance.

Typically, for RFID communication at UHF and higher bands, the antennas employed include loops, slots, and other horizontally polarized antennas [5], [6], [7], [8], [9], [10], [11]. The designers of these antennas have opted for these antenna types for on-body communication due to their simple and low-profile structure. However, since they also run parallel to the skin, these antennas suffer from an overwhelming influence of the body tissues resulting in low efficiency. Acknowledging this, it would be pertinent to consider vertically polarized antenna alternatives.

In this paper, the antenna considered is a variation of a top-loaded monopole, the DDRR antenna [12]. The DDRR is vertically polarized with a miniaturised vertical radiating element connected directly to a tuning transmission line element. For on-body, the DDRR is superior to alternatives such as typical top loaded antennas and PIFA antennas, owing to the simple feed network, critical for tuning to the high permittivity on-body antenna application. The DDRR was originally designed for HF, finding applications on maritime vessels as well with amateur radio enthusiasts. Here, we employ it at UHF for its low-profile vertical radiating element, to run perpendicular to the body and reduce the induced losses. As well as the novel application of the antenna design to on-body, this paper will also demonstrate a new RFID communication package incorporating a framework capable of sending data over 1 kB/s, suitable for applications requiring fast and real-time updates, in this case using accelerometer data [13].

The paper is organised as follows. In Section II the layout of the DDRR is presented, describing the steps to achieve optimal performance through parametric analysis. Then, with the optimal design, an analysis of the antenna bending over expected curvatures for on-body applications is performed. Section III describes the prototyping process for both the antenna and PCB along with the initial practical measurements performed to access the antenna system in real applications. Section IV will then provide a more in-depth analysis of the prototype performance. Followed in Section V with discussion on the system end data acquired from measurements.

Manuscript received 2 August 2022; revised 12 September 2022 and 5 October 2022; accepted 17 October 2022. Date of publication 25 October 2022; date of current version 9 November 2022. This work was supported by the U.K. Engineering and Physical Sciences Research Council under Project EP/P027075/1. *(Corresponding author: Jack D. Hughes.)*

This work involved human subjects or animals in its research. Approval of all ethical and experimental procedures and protocols was granted by the University of Kent Ethics Committee.

The authors are with the School of Engineering, University of Kent, CT2 7NT Canterbury, U.K. (e-mail: jdh23@kent.ac.uk; j.c.batchelor@kent.ac.uk).

This article has supplementary downloadable material available at https://doi.org/10.1109/JRFID.2022.3216762, provided by the authors.

Digital Object Identifier 10.1109/JRFID.2022.3216762

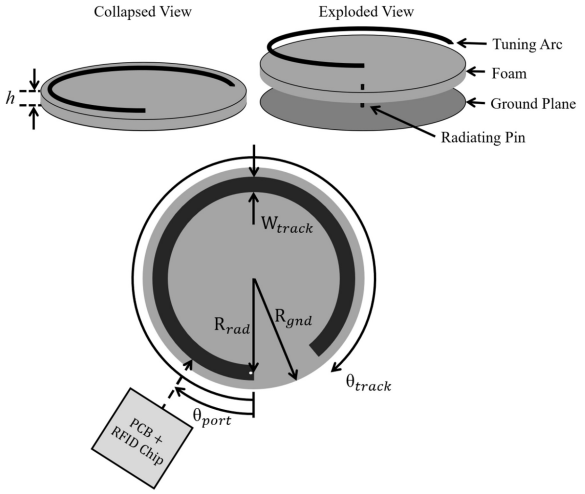

Fig. 1. DDRR Structure: Top transmission line tuning element, EPDM foam layer, ground plane, and a radiating element threading through the foam connecting the top element to the ground plane.

II. Antenna Design and Parametric Analysis

Fig. 1 shows the DDRR structure made up of a ground plane, substrate separator, radiating pin, and transmission line tuning stub. The substrate is a low permittivity foam mounted on a circular ground plane. The height is determined by the foam thickness, thus determining the length of the radiating pin. The arc transmission line and radiating pin (h) combined length is a quarter-wavelength, where the arc circumvents the foam perimeter, acting as the tuning element ($\frac{\lambda}{4} - h$ mm). The radius of the antenna would hence be derived by the location of the vertical radiating element, relative to the centre of the ground plane. There is no significant radiation from the arc transmission line which is parallel and close to the ground plane, meaning the primary radiation element is the vertical feed pin. The resulting structure is low profile, vertically linearly polarised, and orthogonal to the lossy body.

The RFID chip is the EM4325, chosen for its ability to send custom data at a high data rate over an RFID communication link. It was run in battery assisted mode with an input impedance of 7.4 − j122 Ω at 866 MHz, in the microwave simulation environment CST Studio and represented by a discrete port of 7.4 Ω in series with a capacitor of 1.52 pF. All simulations took place on a human body phantom, represented as a 3-layer block model made up of skin, fat, and muscle tissues (Skin $t_{skin} = 1$ mm, $\epsilon_r = 41.6$, $\sigma = 0.9$ S/m, Fat $t_{fat} = 3$ mm, $\epsilon_r = 11.3$, $\sigma = 0.11$ S/m, Muscle $t_{muscle} = 20$ mm, $\epsilon_r = 55.1$, $\sigma = 0.93$ S/m).

To obtain a conjugate match between the DDRR and the chosen RFID IC, the controlling parameters are: the arc length (θ_{track}) and width (W_{track}), radiator pin radius (R_{rad}), ground radius (R_{gnd}), and stub length (θ_{port}). Simulation showed that as the surface area of the capacitive matching element (described by W_{track} and θ_{track}) increased, so did the efficiency. However, since these parameters are factors in determining the antenna match, the resultant efficiency is limited by the ability to tune to 866 MHz. Fig. 2 shows that as W_{track} increases from 6 mm, to 8 mm, to 10 mm the ability to match to the RFID chip is lost, as the θ_{track} cannot extend further without

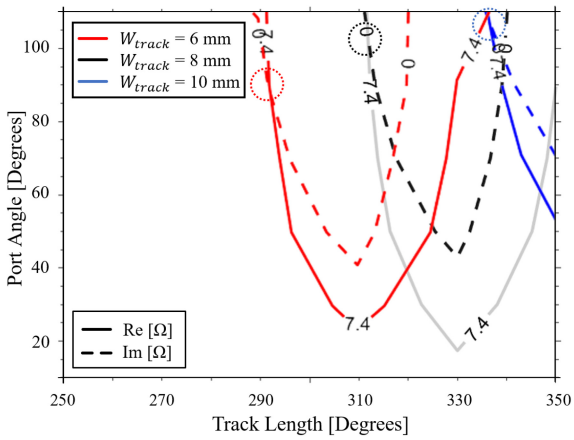

Fig. 2. Complex impedance contour map describing the conjugate match possibilities where the real (solid) line overlaps the imaginary (dashed) line (highlighted by dotted circles) of the DDRR antenna to the RFID IC through parameters θ_{port} and θ_{track}, at $W_{track} = 6$ mm, 8 mm, and 10 mm.

TABLE I
Final Simulated DDRR Parameters (Lengths in *mm*)

h	W_{track}	R_{rad}	R_{gnd}	θ_{port}	θ_{track}
1	8	14	20	105°	312°

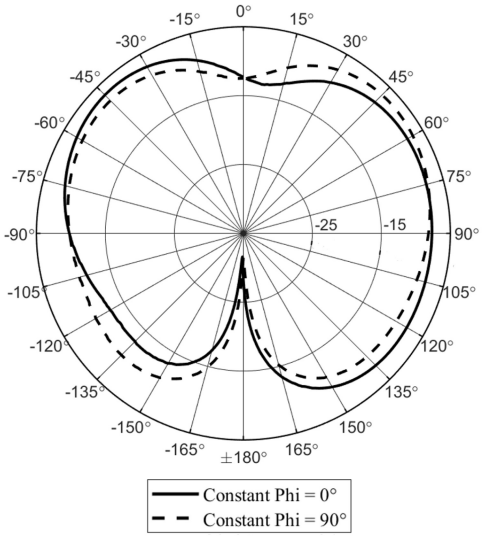

Fig. 3. Simulated radiation pattern of the DDRR on a skin-phantom in the horizontal (Phi = 0°) and vertical plane (Phi = 90°).

overlapping with the start of the loop. Whilst Fig. 2 shows a suitable match for $W_{track} = 10$ mm, it was determined $W_{track} = 8$ mm would be more appropriate as this allows for unaccounted for losses arising in fabrication. Therefore, the matched structure had the following dimensions, shown in Table I. Resulting in an antenna efficiency and gain of $\eta = -9.5$ dBi and G $= -7.5$ dBi. The radiation pattern is shown in Fig. 3.

A. Height Analysis

Having defined the antenna topology, the height can be adjusted to analyse the possible vertical miniaturisation and

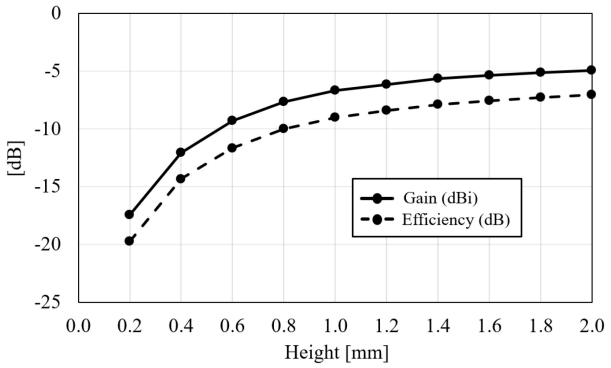

Fig. 4. Simulated DDRR antenna height versus and radiation performance described by gain (solid line) and radiation efficiency (dashed line).

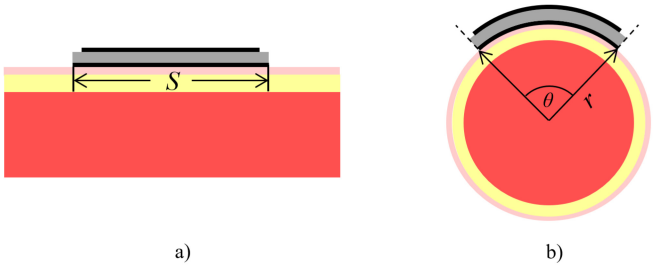

Fig. 5. DDRR antenna simulated structures and 3-layer body model made of skin (pink), fat (yellow), and muscle (red). a) DDRR antenna planar with a flat body model b) DDRR antenna curved around a cylindrical body model.

the relative radiation performance. The height of the antenna is equal to the foam substrate thickness and determines the length of the radiating pin.

Fig. 4, shows how the gain and radiation efficiency change with respect to the DDRR height. Thinner thicknesses show very poor performance capabilities, improving with increased separation until a lower gradient appears from, $h = 1$ mm. Since the ideal antenna for on-body applications would be as low-profile as possible, a verdict must be made on what level of performance is acceptable for the application. Balancing antenna thickness with performance, hence, $h = 1$ mm was deemed an acceptable length reducing the gain by 3 dBi from the maximum.

B. Bending Analysis

The antenna matching simulations were carried out on a flat human-body model. In real applications, the antenna must be flexible to conform with the body. In this section, we assess the ability of the DDRR to bend around a curve, representative of human limbs, whilst maintaining acceptable radiation performance.

The major effect of bending on the antenna is the detuning of the resonant frequency. Since the DDRR is a narrow-band antenna, this affect could be significant to the performance within the ISM UHF band. The antenna bending has been characterized by the bending angle described in (1). The arc angle theta is defined by bending the DDRR over a cylinder with a radius of 'r,' relative to 'S' representing the diameter of the ground plane.

$$S = \theta \cdot r \tag{1}$$

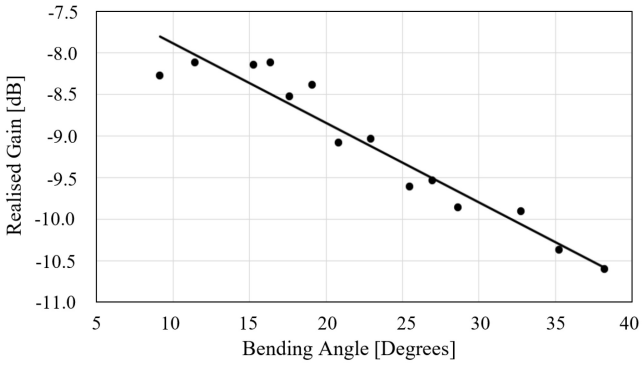

Fig. 6. Simulated DDRR antenna realized gain performance over simulated bending angles until reduced below the lower limit of -10.6 dBi.

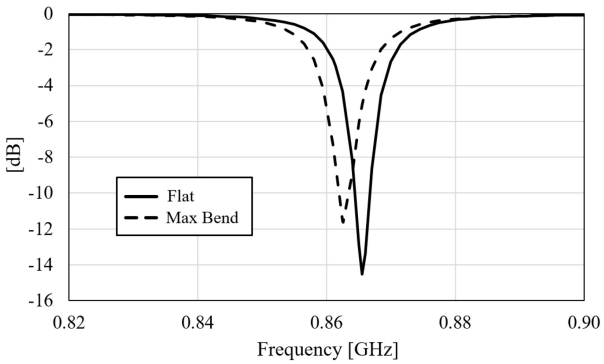

Fig. 7. S11 characteristics, solid line describing the DDRR antenna on the flat body-model, dashed line describing the detuning effect of the maximum allowed bending.

The acceptable performance limit of the antenna under bending is defined by a realized gain reduction of 3 dB with respect to the flat antenna. The flat version saw a realised gain performance of -7.6 dBi, thus, a self-applied realized gain limit of -10.6 dBi is set.

Through CST simulation, the realised gain is seen to decline steadily as bending angle increases (Fig. 6). Using a linear regression line, it can be seen the -10.6 dBi limit is surpassed after 38-degrees of curvature. As expected, the tolerance for curvature is small owing to the narrow bandwidth. However, the body features many acceptable areas that are within the range of this 38-degree 'maximum bend' threshold, such as the side of the arm, back of the hand, thighs, back, torso, and forehead. The respective S_{11} detuning of about 4 MHz and causes the on-frequency (866 MHz) reflection coefficient value to be about -5 dB (Fig. 7).

C. Performance Comparison

The performance and system factors simulated and adopted for this paper are compared with other on-body designs from the literature in Table II. To fairly compare this diverse range of antenna topologies, considered characteristics include substrate, surface area, thickness, radiation properties, RFID chip choice, and RFID reader. Some authors have taken advantage of material dielectrics to reduce the operational wavelength, utilizing materials such as FR-4 or Rogers substrates to allow for a reduction in the size of the antenna at the cost of

TABLE II
SIMULATED RADIATION PERFORMANCE OF ON-BODY UHF RFID ANTENNAS IN LITERATURE

	Antenna Topology	Substrate	Flexible (Y/N)	Area (mm^2)	Thickness (λ)	η (dBi)	Gain (dBi)	RFID Chip
[14]	CP Patch	EPDM	N	50x50	0.014λ	-13.8	-7.1	NXP G2iL
[5]	Slotted Patch	Rogers RT/Duroid 6010LM	N	90x42	0.0116λ	-7	-	Various
[6]	Wire	Polyurethane	Y	30x30	0.00003λ	-	-13	Magnus S3
[7]	Loop (Battery Assisted)	Kapton	Y	30x30	0.00014λ	-	-16.5	AMS-SL900A
[8]	Nested-Slotline	Tattoo	Y	65x20	0λ	-20.7	-16.5	NXP G2X
[9]	Loop	EPDM	Y	23x23*	0.0056λ	-10	-8.7	Alien Higgs 3
[9]	‘’	‘’	‘’	22x22*	0.0028λ	-11	-9.7	‘’
[9]	‘’	Paper	‘’	21x21*	0.00028λ	-16	-14	‘’
[10]	Slotted Patch	FR-4	N	120x30	0.00434λ	-4.3	-	NXP G2XL
[11]	Nested-Slotline	Mylar	Y	105x20	0.00017λ	-	-16	EM4325
This work	DDRR	Foam	Y	40x40*	0.0028λ	-9	-7.5	EM4325

**Circular antenna shape*

being rigid materials. Other authors have attempted to maximise radiation performance whilst limiting themselves to the ‘epidermal’ definition, choosing groundless topologies with ultra-thin substrates, such as polyurethane. Relatively speaking, the thicker and more obtrusive the substrate is, the greater the performance gain, and the lower the profile and more body conformal the antenna is, the worse the radiation performance. The DDRR parameters are selected between the extremes and in comparison to the antennas in Table II, the design does not obtain the smallest area or thinnest thickness, such of that of [6] or [9], but the radiation performance achieved relative to the size, with being on a flexible material, does provide improvements in gain and efficiency over alternatives such as [14], and the EPDM versions of [9].

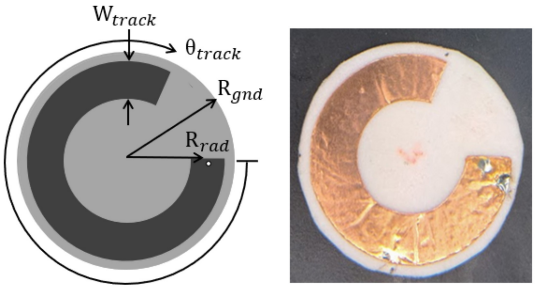

Fig. 8. DDRR antenna line drawing and prototype, dimensions given in Table I.

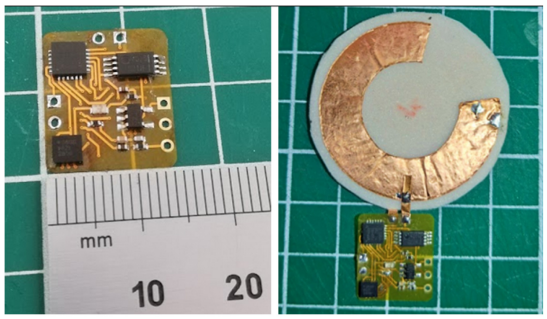

a) b)

Fig. 9. Kapton PCB a) size b) connection to DDRR antenna via short copper tracks at θ_{port}, given in Table I.

III. TAG PROTOTYPING

A. DDRR Antenna Prototype

The DDRR was prototyped using a ‘Cricut’ die cutter. Using adhesive copper tape, the two sides of the DDRR antenna were cut to size, producing the tuning circuit and ground plane. For the substrate, foam (ROHACELL HF) was utilised for the soft and flexible structural properties with a dielectric closely resembling air [15]. Once the copper layers were adhered to the foam, a 0.2 mm diameter wire is slotted through a pin hole, soldered, then trimmed to size for the radiating element. The resultant structure is shown in Fig. 8.

B. Kapton PCB

The Kapton PCB designed for this system (Fig. 9 a) is an application specific flexible board for the power and size constrained domain of sending data to a host PC via UHF RFID. One of the main requirements of the board is ultra-low power operation for battery longevity. To achieve this, the MSP430FR2433 microcontroller unit (MCU) from Texas

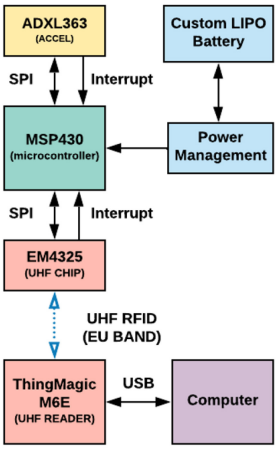

Fig. 10. System component interconnection and communication flowchart.

Instruments is employed together with the EM4325 RFID transponder and the low power ADXL363 accelerometer from Analog Devices. The latter provides relative orientation to 'x,y,z' axes. In addition to the accelerometer data, the MCU has been coded to increment an integer with each RFID IC interruption by the RFID reader (between 0 and 255 before resetting). Thus, when a data packet fails to send, the integer value increments to indicate data has been lost. In operation, the EM4325's auxiliary pin is used by the MCU as an interrupt to schedule loading the data into the EM4325's RAM register, allowing for high speed read out communication with minimal corruption. The complete system interconnections from the components on the PCB communicating through the antenna are shown in Fig. 10.

C. Tag Construction

Using the simulation dimensions as a guide, short copper foil tracks were soldered between the kapton PCB and antenna linking the tuning track and ground plane to define the angle, θ_{port} (Fig. 9 b). Adjusting θ_{port} in combination with trimming the length θ_{track} with a scalpel, the antenna could be tuned for optimum performance at 866 MHz. To determine the frequency response and gauge performance between adjustments, a Voyantic Tagformance Pro was utilised using the read range measurement setting. The DDRR tag was attached to the upper right arm with microporous surgical tape, Fig. 11 shows the arm mounted tag on double-sided adhesive tape to more clearly display structure, the surgical tape is more straightforward to remove from the skin. Once mounted, the tag was positioned at a calibrated distance of 30cm from the Voyantic reader antenna, so the frequency response could be measured, as shown in Fig. 12. Alternative reader positions directly above and below the arm were also tested, however the most prominent beam was clearly pointing broadside to the tag antenna. The final tuned prototype DDRR parameters are shown in Table III.

IV. Tag Performance Measurements

The radiation pattern cannot be measured in a conventional manner since the antenna complex impedance would require a matching network which effects the radiation performance,

TABLE III
Final Prototype DDRR Parameters (Lengths in *mm*)

h	W_{track}	R_{rad}	R_{gnd}	θ_{port}	θ_{track}
1	8	14	20	85°	210°

Fig. 11. DDRR tag placement on the upper right arm attached via double sided tape.

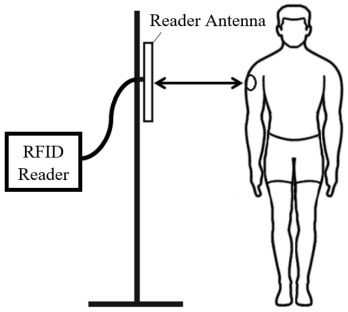

Fig. 12. DDRR tag performance measurement with RFID reader setup.

therefore returning the DDRR to 50 Ω would not be comparable to the RFID matched performance. Instead, the antenna radiation performance and radiation pattern are assessed practically, through the quality of the communication link relative to body position. The attachment of the tag to the body plays a role in how the orientation of the radiation beam will be received by the reader antenna, circularly polarized. For ease of use, the orientation of the tag was kept such that the kapton PCB and battery were always aligned along the arm as shown in Fig. 11. Measurements were performed using the 'ThingMagic M6e' RFID reader, chosen for the fast read rate, intuitive software development kit (SDK), and availability.

For initial measurements, the worn DDRR tag was moved away from the reader antenna in 5 cm increments, maintaining a 'static' body position as described by Fig. 12, until the maximum read distance was found, and the results are presented in Fig. 13. In this application, 32 bits of data are being passed over the communication link, 24 bits for the accelerometer data (8 bits per axis) and 8 bits for the counter. As such, when communicating at full speed, over 250 reads per second, the data rate is 8 kbps (250 reads · 32 bits), equating to 1 kBps. Data dropouts are observed between 2.1 m and 3 m, are likely caused by channel effects including constructive and destructive interference in a complex echoic environment. Although reads are obtainable at 180, 300, 350, and 380 cm, in practice the maximum read range is 120 cm. Further investigation using antenna diversity at the reader could help extend the read range.

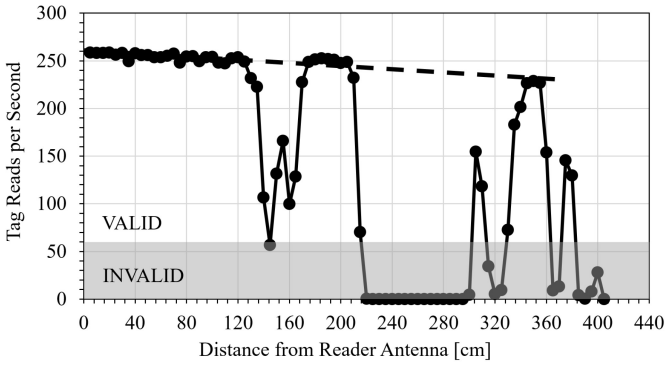

Fig. 13. Data rate measurements taken in 5cm increments from the reader antenna, dashed line represents data fall off with distance for the unfaded signal. Grey area indicated unacceptable data rate.

TABLE IV
EXAMPLE ACCELEROMETER DATA FROM THE TAG

Time	X	Y	Z	Counter	RSSI
02.36.42.829	56	243	246	136	-65
02.36.42.833	56	243	246	137	-66
02.36.42.836	56	243	246	138	-66
02.36.42.839	56	243	246	139	-65
02.36.42.845	56	243	246	140	-65
02.36.42.848	56	243	246	141	-66
02.36.42.855	56	244	246	143	-65
02.36.42.861	56	244	246	144	-65

The speed of the tag data appears proportional with the read distance, suffering a 30 reads per second decrease between the closest and furthest functional read ranges. However, the grey area representing the minimum acceptable sample rate for medical application (60 Hz), shows the speed is well within acceptance, up to the 2.1 m drop out [16]. The gradient of the unfolded dashed line describes the data rate decreasing at a rate of ∼0.09 reads per second/cm, or ∼1 read/s is lost every 10 cm, when not in a null.

Using the information obtained in the 'static' measurements, the performance of the tag was then considered as the wearer moved, at distances where performance was achieved, namely 50 cm, 100 cm, 200 cm, and 350 cm.

The movements undertaken were designed to best describe the limitations of the antenna with respect to a single reader antenna and be representative of possible therapeutic exercises the tag could be adopted for, described by Fig. 14. For all movements, measurements were taken as before, with respect to the reader antenna, broadside to the tag. In movement cases where a reasonable level of performance was achieved and measurements were taken with the person facing the antenna, as shown in Fig. 15.

The communication link performance has been tested through controlling the data output of the tag. That is, each time the tag is interrogated, the MCU will attempt to send the accelerometer data and a counter, which when received by the host PC, will be timestamped and provide the correlating 'Received Signal Strength Indicator' (RSSI) value of when the data was received, as shown in Table IV.

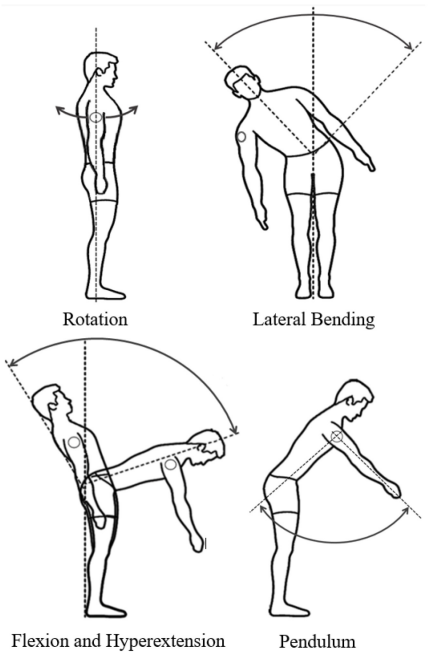

Fig. 14. Movements performed indicating the location of the DDRR antenna on the upper arm.

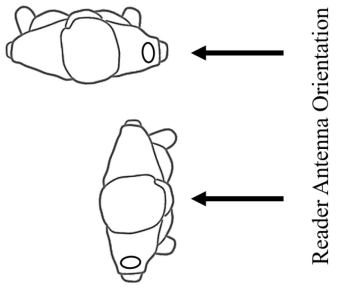

Fig. 15. Relative body orientations of the measurements with the tag facing the reader antenna directly, then the body facing the reader antenna.

Movements took place in a 5 s recording period, at the end of which some statistics were calculated. In the order of events taking place, the first statistic is the 'Total Tag Reads', referring to the total number of times the tag is interrogated by the reader. From which, the number of 'Reads with Data' is found, that is, the number of reads of the tag holding certifiable data, excluding empty or faulty packets. Next, each time the counter value presented did not align with the previous counter (counter $\neq$ previous counter $+$ 1) between 0-255, it is noted that packets have been dropped, thus, they were subtracted from the 'Tag Reads with Data' providing the number of 'Reliable Tag Reads with Data'. An example of this packet loss phenomenon can be seen in Table IV, whereby the counter excludes 142. Finally, the 'Data Reliability' is calculated, with the following formula: ('Reliable Tag Reads with Data' / 'Total Tag Reads') $\times$ 100%. The data presented is the average of three rounds of measurements of each movement, at each distance. The movement data are presented in the following: 'Lateral Bending', Table V; 'Flexion and Hyperextension', Table VI; 'Pendulum', Table VII; and 'Rotation', Table VIII.

Considering the 'Total Tag Reads' of each movement, it would suggest that the biggest range of motion (RoM) can

TABLE V
AVERAGE LATERAL BENDING DATA CAPTURE AND RELIABILITY WHEN THE TAG IS FACING THE READER ANTENNA, THEN THE BODY FACING THE READER ANTENNA

Lateral Bending (Tag Facing Reader Antenna)					
Distance (cm)	**Total Tag Reads**	**Reads with Data**	**Dropped Packets**	**Total Tag Reads with Data**	**Data Reliability**
50	897	848.3	60	788.3	91.9
100	925	885.3	58.3	827	83.0
200	731.3	657	86	571	80.6
350	573	478.6	94.3	384.3	62.7
Lateral Bending (Body Facing Reader Antenna)					
50	1189.3	1150.6	68.3	1082.3	91.0
100	1185.3	1138	71.6	1066.3	89.9
200	970.6	840.3	118	722.3	74.4
350	348.3	250.6	97.6	153	43.9

TABLE VI
AVERAGE FLEXION AND HYPER-EXTENSION BENDING DATA CAPTURE AND RELIABILITY WHEN THE TAG FACING THE READER ANTENNA, THEN THE BODY FACING THE READER ANTENNA

Flexion to Hyperextension (Tag Facing Reader Antenna)					
Distance (cm)	**Total Tag Reads**	**Reads with Data**	**Dropped Packets**	**Total Tag Reads with Data**	**Data Reliability**
50	1154	1089	92	997	86.4
100	834.6	790	62.6	727.3	87.1
200	879.6	667.6	185.3	482.3	54.8
350	577.6	456	140	316	54.7
Flexion to Hyperextension (Body Facing Reader Antenna)					
50	1277	1232.6	76	1156.6	90.5
100	1090	982	107.3	874.6	80.2
200	590	463.6	110.3	353.3	59.9
350	0	0	0	0	0

TABLE VII
AVERAGE PENDULUM MOVEMENT DATA CAPTURE AND RELIABILITY WITH THE TAG FACING THE READER ANTENNA

Pendulum					
Distance (cm)	**Total Tag Reads**	**Reads with Data**	**Dropped Packets**	**Total Tag Reads with Data**	**Data Reliability**
50	1189	1091.6	115	976.6	82.1
100	1188.3	1153.3	75.3	1078	90.7
200	1162.3	1079	107	972	83.6
350	918.3	783.3	155	628.3	68.4

be detected at the closest distance, evident from the data rate being consistently highest. Also suggesting, that as the distance increases, the ability to transmit data consistently at high speed becomes more difficult, thus, less of the movement is communicated. However, the 'Data Reliability' percentage suggests in the measurement environment (3.8 m × 6.5 m × 2.5 m, reader antenna at tag height 1.35 m above the floor) in many cases the optimum distance for detecting maximum RoM is 1 m, where fewer, but more reliable packets are received, while decaying at longer distances. Whilst it is difficult to compare the radiation pattern between the simulated

TABLE VIII
AVERAGE ROTATION MOVEMENT DATA CAPTURE AND RELIABILITY WITH THE TAG FACING THE READER ANTENNA

Rotation					
Distance (cm)	**Total Tag Reads**	**Reads with Data**	**Dropped Packets**	**Total Tag Reads with Data**	**Data Reliability**
50	897	848.3	60	788.3	87.9
100	925	885.3	58.3	827	89.4
200	731.3	657	86	571	78.1
350	573	478.6	94.3	384.3	67.1

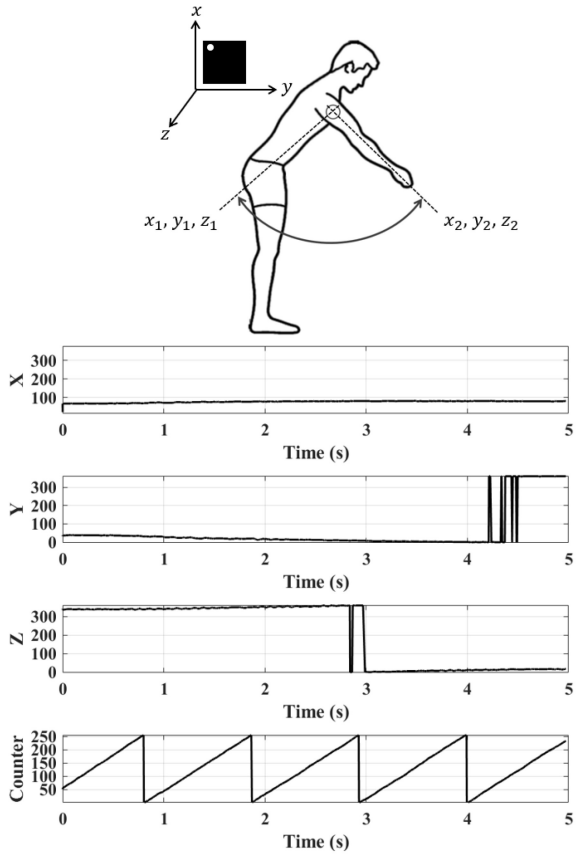

Fig. 16. ADXL363 accelerometer orientation when worn on the arm and raw received accelerometer axis data (0°- 360°) and counter data (0 - 255) of the Pendulum movement at 50cm.

pattern and the tabulated data, the measured results do indicate the main beam direction to be broadside of the antenna, however more narrow in beam width.

V. DATA PROCESSING

Fig. 16 displays the raw data seen on each axis of the accelerometer throughout the 5 second motion of the 'Pendulum', at 50 cm read distance. Each axis wraps between 0°and 360°, causing spikes to appear (Y axis: 4.2 s − 4.5 s and Z axis: 2.8 s − 3 s) where the axis value is transitioning over this threshold. Whilst the total change in each axis value is subtle, this shows the capability for accurate body movement detection, or adoption of other sensors requiring sensitivity to variation.

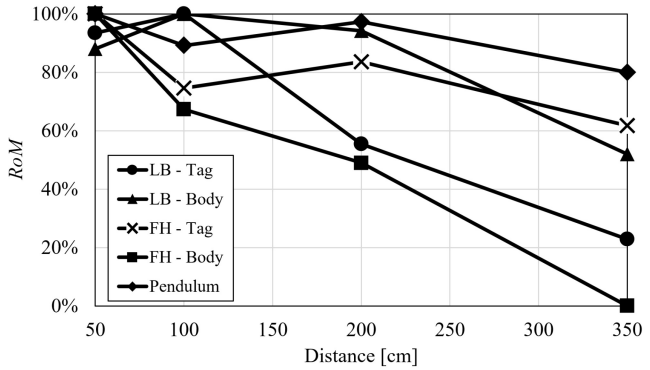

Fig. 17. Relative range of motion detectable of each movement at the read distances 50cm, 100cm, 200cm, and 350cm.

To quantify the range of movement that can be captured by the tag at a given read distance, the results in Tables V–VII are represented as a Range of Motion (RoM). The maximum range of each movement (averaged over 3 repetitions) between the start point $x_1, y_1, z_1 = x(t=0), y(t=0), z(t=0)$ and end point $x_2, y_2, z_2 = x(t=5\,\text{s}), y(t=5\text{s}), z(t=5\text{s})$ is compounded into a single value called RoM as described by (2)–(5).

$$\Delta x \equiv x_2 - x_1 \pmod{255} \tag{2}$$

$$\Delta y \equiv y_2 - y_1 \pmod{255} \tag{3}$$

$$\Delta z \equiv z_2 - z_1 \pmod{255} \tag{4}$$

$$RoM = \Delta x + \Delta y + \Delta z \tag{5}$$

The RoM value was then normalised into a percentage with respect to highest RoM value found over all distances, resulting in Fig. 17. 'Rotation' is excluded since this movement was a spinning motion around the torso axis maintaining the arm parallel to said axis of rotation, thus, the accelerometer axis data does not change. From the accelerometer results, it can be seen that the best range of motion data is received at either 50 cm or 100 cm, however in the movements where the motion is favourable to the antenna orientation, namely the pendulum movement as the tag is maintained well within the reader antenna beam, the performance even at the maximum ranges are reasonably reliable.

Whilst this system is only utilising 32 bits, the full capability of the EM chip is 128 bits which is accessible without impact on the speed. The speed at which the reader antenna is interrogating the tag antenna is significantly faster than the sensor is capable of updating, therefore, the RFID platform could support higher data rate sensors.

VI. Conclusion

A thin, soft, flexible UHF RFID tag vertically polarised with respect to its ground plane has been designed and fabricated for the application of on-body wireless sensing. The results presented indicate the tag is suitable for the tracking of body movements when the tag wearer is within a 2.1 m proximity of the reader antenna, with further read range achievable for data transmission under select body orientations. The speed at which the data is communicated would be suitable for real applications in the transmission of sensor data from the body, achieved with ultra-low-power operations. The antenna performance is competitive with other reputable antenna topology types, obtaining a higher efficiency and gain than those of similar size. For future development of the tag, the next suggested step is to replace the coin cell battery with a thinner, more flexible battery, to allow for a more integrated antenna, PCB, and battery tag [11]. For application, it is recommended that reader antenna diversity is adopted to account for multipath interference nulls. Whilst adding a secondary reader antenna would halve the average data rate over the communication link to a single reader, the performance capability shown in this paper is significantly above twice the minimum acceptable sample speed. Other improvements could be achieved by adopting more recent reader technology that offers higher sensitivities than the M6e [17].

References

[1] G. M. Bianco, C. Occhiuzzi, N. Panunzio, and G. Marrocco, "A survey on radio frequency identification as a scalable technology to face pandemics," *IEEE J. Radio Freq. Identif.*, vol. 6, pp. 77–96, 2022, doi: 10.1109/JRFID.2021.3117764.

[2] C. Occhiuzzi, S. Parrella, F. Camera, S. Nappi, and G. Marrocco, "RFID-based dual-chip epidermal sensing platform for human skin monitoring," *IEEE Sensors J.*, vol. 21, no. 4, pp. 5359–5367, Feb. 2021, doi: 10.1109/JSEN.2020.3031664.

[3] D. H. Kim et al., "Epidermal electronics," *Science*, vol. 333, no. 6044, pp. 838–843, 2011, doi: 10.1126/science.1206157.

[4] X. Li, G. Gao, H. Zhu, Q. Li, N. Zhang, and Z. Qi, "UHF RFID tag antenna based on the DLS-EBG structure for metallic objects," *IET Microw. Antennas Propag.*, vol. 14, no. 7, pp. 567–572, 2020, doi: 10.1049/iet-map.2019.0780.

[5] G. A. Casula, G. Montisci, G. Valente, and G. Gatto, "A robust printed antenna for UHF wearable applications," *IEEE Trans. Antennas Propag.*, vol. 66, no. 8, pp. 4337–4342, Aug. 2018.

[6] C. Miozzi, F. Amato, and G. Marrocco, "Performance and durability of thread antennas as stretchable epidermal UHF RFID tags," *IEEE J. Radio Freq. Identif.*, vol. 4, pp. 398–405, 2020.

[7] C. Miozzi, S. Nappi, S. Amendola, and G. Marrocco, "A general-purpose small RFID epidermal datalogger for continuous human skin monitoring in mobility," in *IEEE/MTT-S Int. Microw. Symp. Dig. Tech.*, 2018, pp. 371–373, doi: 10.1109/MWSYM.2018.8439572.

[8] M. A. Ziai and J. C. Batchelor, "Temporary on-skin passive UHF RFID transfer tag," *IEEE Trans. Antennas Propag.*, vol. 59, no. 10, pp. 3565–3571, Oct. 2011, doi: 10.1109/TAP.2011.2163789.

[9] P. S. Taylor and J. C. Batchelor, "Finger-worn UHF far-field RFID tag antenna," *IEEE Antennas Wireless Propag. Lett.*, vol. 18, pp. 2513–2517, 2019, doi: 10.1109/LAWP.2019.2941731.

[10] A. Dubok and A. B. Smolders, "Miniaturization of robust UHF RFID antennas for use on perishable goods and human bodies," *IEEE Antennas Wireless Propag. Lett.*, vol. 13, pp. 1321–1324, 2014, doi: 10.1109/LAWP.2014.2337051.

[11] M. C. Caccami, M. P. Hogan, M. Alfredsson, G. Marrocco, and J. C. Batchelor, "A tightly integrated multilayer battery antenna for RFID epidermal applications," *IEEE Trans. Antennas Propag.*, vol. 66, no. 2, pp. 609–617, Feb. 2018, doi: 10.1109/TAP.2017.2780899.

[12] R. C. Hansen and R. E. Collin, "Clever physics, but bad numbers," in *Small Antenna Handbook*. Hoboken, NJ, USA: Wiley, 2011, ch. 4, pp. 135–145, doi: 10.1002/9781118106860.

[13] R. Horne and J. C. Batchelor, "A framework for a low power on body real-time sensor system using UHF RFID," *IEEE J. Radio Freq. Identif.*, vol. 4, pp. 391–397, 2020, doi: 10.1109/JRFID.2020.3018405.

[14] D. Le, S. Ahmed, L. Ukkonen, and T. Björninen, "A small all-corners-truncated circularly polarized microstrip patch antenna on textile substrate for wearable passive UHF RFID tags," *IEEE J. Radio Freq. Identif.*, vol. 5, pp. 106–112, 2021, doi: 10.1109/JRFID.2021.3073457.

[15] "ROHACELL HF foam material." Accessed: Oct. 10, 2022. [Online]. Available: https://performance-foams.evonik.com/en/products-and-solutions/rohacell/rohacell-hf-170037.html

[16] R. Horne, P. Jones, P. Taylor, J. Batchelor, and C. Holt, "An on body accelerometer system for streaming therapy data using COTS UHF RFID," in *Proc. IEEE Int. Conf. RFID Technol. Appl. (RFID-TA)*, Pisa, Italy, 2019, pp. 301–305, doi: 10.1109/RFID-TA.2019.8892220.

[17] "Impinj R700 RAIN RFID reader for enterprise-grade IoT solutions." Accessed: Oct. 10, 2022. [Online]. Available: https://www.impinj.com/products/readers/impinj-r700